Mathematical Biosciences and Engineering

MBE, 17(4): 3088–3108.
DOI: 10.3934/mbe.2020175
Received: 30 December 2019
Accepted: 07 April 2020
Published: 15 April 2020

http://www.aimspress.com/journal/MBE

Research article

Retinal blood vessel segmentation based on Densely Connected U-Net

Yinlin Cheng[1,3,†], Mengnan Ma[1,3,†], Liangjun Zhang[1], ChenJin Jin[2], Li Ma[2], Yi Zhou[3,*]

[1] School of Biomedical Engineering, Sun Yat-sen University, Guangzhou 510006, China
[2] Zhongshan Ophthalmic Center, Sun Yat-sen University, Guangzhou 510006, China
[3] Department of Medical Informatics, Zhongshan School of Medicine, Sun Yat-sen University, Guangzhou 510006, China

† These authors contributed equally to this work.

*** Correspondence:** Email: zhouyi@mail.sysu.edu.cn; Tel: 02087332139.

Abstract: The segmentation of blood vessels from retinal images is an important and challenging task in medical analysis and diagnosis. This paper proposes a new architecture of the U-Net network for retinal blood vessel segmentation. Adding dense block to U-Net network makes each layer's input come from the all previous layer's output which improves the segmentation accuracy of small blood vessels. The effectiveness of the proposed method has been evaluated on two public datasets (DRIVE and CHASE_DB1). The obtained results (DRIVE：Acc = 0.9559，AUC = 0.9793，CHASE_DB1：Acc = 0.9488，AUC = 0.9785) demonstrate the better performance of the proposed method compared to the state-of-the-art methods. Also, the results show that our method achieves better results for the segmentation of small blood vessels and can be helpful to evaluate related ophthalmic diseases.

Keywords: retinal fundus image; U-Net; blood vessel segmentation; neural networks; dense block

1. Introduction

Diabetic Retinopathy (DR) is the most common diabetic eye disease which might cause vision loss [1]. According to the World Health Organization, more than 347 million people have diabetes around the world, and the number of people with diabetes is expected to reach 439 million by 2030 [2]. Retinopathy screening has important clinical significance for early prevention and timely treatment of diabetic patients. Retinopathy screening is used to assess and monitor various ophthalmic diseases, delay the patient's condition and reduce the risk of blindness [3]. In order to facilitate the diagnosis of

retinal fundus and other related diseases, accurate segmentation of retinal blood vessels is required. However, fundus images have some problems such as the possible bleeding points, the exudation, the centerline reflection and the low contrast microscopic blood vessels. Those problems make the blood vessel segmentation of fundus images always a hot issue around the world.

For the past few years, many algorithms and models in retinal blood vessel segmentation are proposed. According to whether need a prior marked information, the algorithm can be divided into two types: Unsupervised learning method [4–8] and supervised learning method [9–13]. Unsupervised methods attempt to find the intrinsic pattern of blood vessels in retinal images and then use this pattern to determine if a particular pixel belongs to a blood vessel. On the contrary, supervised methods are usually based on supervised machine learning algorithms by using the training set of marked retinal images to learn the rules of blood vessel segmentation.

Unsupervised learning does not require manually annotated images as a priori marker information, and uses the similarities between the data for analysis. Such as Chaudhuri et al. [14], proposed a matched filtering algorithm. The algorithm can detect blood vessels in 12 different directions, then calculate the threshold result, and outputs the maximum response result. This method utilizes the optical and spatial characteristics of blood vessels to extract retinal blood vessels. Though it achieves high accuracy, but cannot extract small blood vessels accurately. The same example as capillaries. Zana et al. [15], proposed a method based on mathematical morphology and curvature assessment to segment blood vessels from retinal images. But this algorithm relies on structural elements too much. Also Fraz et al. [16], used vascular centerline and morphological method to extract vascular trees from retinal images, but longer extraction time.

Compared with the unsupervised learning method, supervised learning method uses manually annotated images as training dataset label to generate corresponding algorithm models. Staal et al. [11], proposed a method to calculate eigenvector for each pixel based on the ridge line of the retina image, and then used k-Nearest Neighbors (KNN) algorithm and sequence forward feature selection algorithm to classify the feature vector. Jiang et al. [17], proposed a new blood vessel segmentation method based on pre-trained Fully Convolutional Networks (FCN). This method combined the full-size image segmentation results into the regional blood vessel pixel segmentation results to improve the accuracy and robustness of the algorithm. Though those algorithms get a good result, but still have some downsides.

U-Net network structure is a deep learning architecture proposed by Ronneberger et al. [18] in 2015, which greatly promotes the research of medical image segmentation. U-Net network consists of two parts: Contracting path [18], using "Conv + Pooling" for subsampled to obtain context information; Symmetric Expanding path [18], using "Deconv" for upsampling to obtain precise position. U-Net network structure is widely used in medical image segmentation and performs well, Oktay et al. [19] demonstrate the implementation of attention gate (AG) in a standard U-Net architecture (Attention U-Net) and apply it to medical images，the model is evaluated on two large CT abdominal datasets. Rundo et al. [20] proposed the USE-Net, which incorporates Squeeze-and-Excitation (SE) blocks into U-Net, the model is evaluated on three T2-weighted MRI datasets and have a good performance. For the field of retinal blood vessel segmentation, Wang et al. [21], proposed a U-shaped network method based on convolutional neural network to segment the fundus image vessels. Kumawat et al. [22], proposed a fundus segmentation algorithm based on the local U-shaped network, and had achieved a good segmentation effect.

In addition, many other supervised methods [23–25] have been proposed. The segmentation

accuracy of the above supervised learning methods is superior to unsupervised learning methods. But the proposed algorithms also have some shortcomings, such as the inability to accurately segment small blood vessels and the poor robustness of the algorithm.

This algorithm which proposed on the basis of traditional U-Net network, is optimized to further improve the segmentation accuracy of small blood vessels. Based on the full understanding of the characteristics of retinal fundus color image and the latest algorithm model, we proposed a new method of blood vessel segmentation, Dense U-Net model. In Dense U-Net model we replace the convolution layers of U-Net with dense block modules. In addition, we use Parametric Rectified Linear Unit (PReLU) [26] as the activation function of the dense block to improve our model's fitting and generalization capabilities. Our model is used to accomplish the accurate segmentation of small blood vessels in retinal images, and to further improve the accuracy and sensitivity of blood vessel segmentation. Compared with the existing methods, our method has a significant improvement in sensitivity while maintaining the same segmentation accuracy, which is of great clinical significance for determining the diagnosis of neovascularization and microaneurysm in patients. Our algorithm model proposed in this study is tested on the public datasets: Digital Retinal Images for Vessel Extraction (DRIVE) [27] and CHASE_DB1 [28], and obtains a better segmentation performance, which can prove the feasibility of our algorithm.

The other sections of this paper are organized as follows, the second section introduces the related work, the third section introduces our proposed method, the fourth section introduces our experimental results and discussion, and the fifth section introduces our conclusions.

2. Related works

Retinal fundus vascular image segmentation has received more and more attention in image processing. There are a large number of methods have been proposed for the segmentation of vessels in retinal images, which can be divided into two categories: Unsupervised and supervised.

Supervised learning uses manual segmentation images by experts as labels for training data to generate corresponding algorithm models. The manual segmentation images are also used to compare with the predicted results of the artificial intelligence algorithm to evaluate the algorithm model. Unsupervised learning does not require labels, which analyzes the similarities between a large number of retinal images. It is also more widely used than supervised learning.

To automatically segment blood vessels in fundus images of the retina, Calimeri et al. for the first time proposed to use a neuroevolution method named Hypercube NeuroEvolution of Augmenting Topologies (HyperNEAT) [29]. It had reached a good segmentation performance in the DRIVE and STARE data set. Although this model is simple-structured, it can achieve higher accuracy when segmenting biomedical-related images.

2.1. Unsupervised methods

The unsupervised methods can be classified into four main subcategories: Matched filter, vessel tracking, mathematical morphology and model-based approaches. A typical unsupervised learning algorithm workflow is shown in Figure 1. During model tuning, the goodness of the model is evaluated and the model is tuned according to a minimization function that aims at finding the best separation between the vascular and background classes [1].

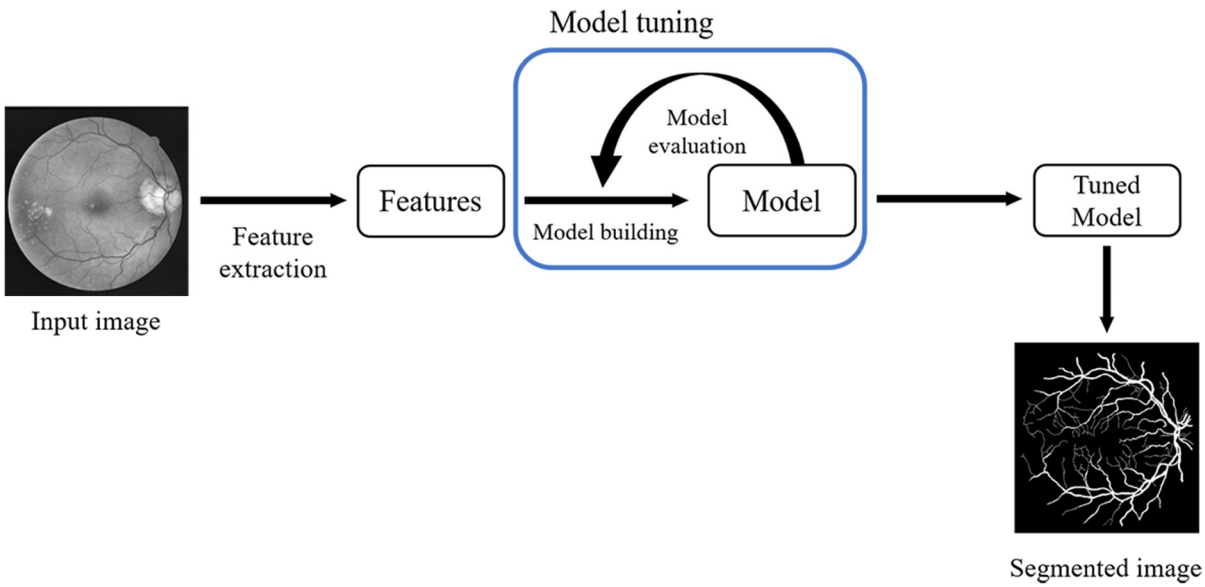

Figure 1. Unsupervised learning algorithm workflow based on unlabeled image features.

For the methods based on matched filter, it convolves a 2-D kernel with the retinal image. Chaudhuri et al. constructed 12 different templates that are used to extract feature of retinal images based on the optical and spatial properties of blood vessel, and the maximum response of matched filter was retained. Compared to other methods, the proposed method retains the computational simplicity of edge operators, and incorporates the advantages of using model-based edge detectors. Matched filter (MF) has achieved better accurate results in blood vessel detection, but it might not recover all the vessel, like capillaries. In order to overcome the deficiency of the MF, Cinsdikici et al. [30] proposed a hybrid model of matched filter and ant colony algorithm named MF/ant algorithm. Using MF/ant algorithm in DRIVE database, the average ROC area and maximum accuracy average are 0.9407, 0.9293. Another example is as follows [31], Sreejini et al. proposed particle swarm optimization for finding the optimal filter parameters of the multiscale Gaussian matched filter for achieving improved accuracy of retina vessel segmentation. The average accuracy, sensitivity and specificity are 0.9633, 0.7132 and 0.9866, respectively, on the DRIVE database and 0.95, 0.7172 and 0.9687 for the STARE database. In addition, several different algorithms were developed based on matched filter [32,33].

Vessel tracking based methodology [34], Vlachos et al. proposed multi-scale single channel line-tracking algorithm. By tracking the centerline of the vessel, the entire vascular network is mapped after edge detection. This method relies on the results of edge detection and takes a long time to obtain the vessel network. Quek and Kirbas [35] proposed the wave propagation and trackback method, using local information to extract the vasculature. This method allows to extract not only the individual vessels, but the vascular connection morphology as well. The model based approaches include the vessel profile models [36,37], deformable models [38], to extract the retinal vessels.

In mathematical morphology, Zana and Klein [15] proposed an algorithm based on mathematical morphology and curvature evaluation for blood vessels segmentation. Fraz and Barman [16] presented a novel method, which combines vessel centerlines detection and morphological bit plane slicing to extract the blood vessel tree from the retinal images, but the segmentation time required was longer.

2.2. Supervised methods

In supervised methods, the segmentation algorithm needs to acquire the rule for vessel segmentation by learning the images that are manually labeled by experts. The workflow of a typical supervised approach is shown in Figure 2. During the training phase, image features are extracted from the training images as the feature vectors. A machine learning model acquires necessary knowledge by trained with feature vectors and the corresponding labels, taken from the Gold Standard segmentation. While the model is trained, it can be applied to a new, unseen, testing image to obtain the vessel segmentation.

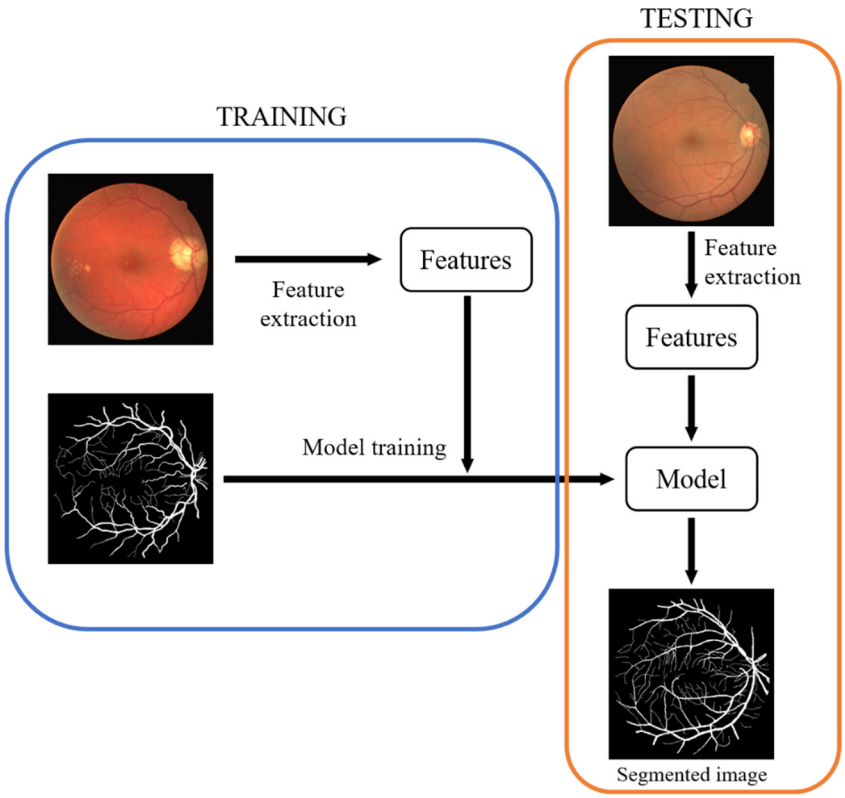

Figure 2. Supervised approach workflow.

For instance, Staal et al. [11] proposed the algorithm for retinal vessel segmentation based on segmentation of images ridges. For every pixel, using the algorithm to compute the feature vectors, then the feature vectors are classified using a KNN classifier and sequential forward feature selection. The average accuracy is 0.9516 and an area under the ROC curve is 0.9614 on the STARE database.

Soares et al. [10] proposed a method also based on the pixel's vector. Authors use the pixel's intensity and two-dimensional Gabor wavelet transform responses taken at multiple scales as the feature vectors. Then use Bayesian classifier with class-conditional probability density functions described as Gaussian mixtures to classify each pixel as either a vessel or non-vessel pixel. The method achieves an average accuracy of 0.9466 and 0.9480 and the area under the ROC curve as 0.9614 and 0.9671 for DRIVE and STARE, respectively.

In addition, Wang et al. [24] proposed a new convolutional network architecture and apply deep

learning based on U-Net convolutional network for real patients' fundus images. The accuracy of the proposed method on DRIVE is 0.9790. Jiang et al. [17] based on a pre-trained fully convolutional network through transfer learning proposed a supervised method. They use this method make retinal vessel segmentation easier from full-size image segmentation to regional vessel element recognition and result merging. Meanwhile, using additional unsupervised image post-processing techniques to refine the final result. The methodology is evaluated on the DRIVE, STARE and CHAES_DB1 datasets resulting in an average accuracy of 0.9624, 0.9734, 0.9668, the area under the ROC curve as 0.9810, 0.9900, 0.9810, the sensitivity as 0.7540, 0.8352, 0.8640, and the specificity as 0.9825, 0.9846, 0.9745 for DRIVE, STARE and CHASE_DB1, respectively. There are many other supervised methods such as Xu [23], Wang [24], Soomro et al. [25].

3. Proposed methods

In the following, pre-processing methods upon retinal fundus images would be firstly introduced, including grayscale, Z-score, Contrast Limited Adaptive Histogram Equalization (CLAHE) [39], and gamma correction. Then, we introduced the architecture of U-Net and dense block. Finally, we proposed an improved U-Net network model and its parameter settings.

3.1. Pre-processing

Before training, there is a required pre-processing step. The goal of the step is to make the model a higher learning efficiency. Many methods have been proposed for medical image preprocessing, for example the MedGA proposed by Rundo et al. [40]. MedGA is a novel evolutionary method for image enhancement in medical image processing, which can be exploited as a pre-processing step for the enhancement of images with an approximate bimodal histogram distribution. Zhou et al. [41] proposed a new image enhancement method to improve color retinal image luminosity and contrast. The proposed method is shown to achieve a superior image enhancement, while simultaneously preserving image naturalness. Retinal image data is used to a large number of early pathological tests. However, the poor brightness, low contrast, and poor ambiguity of retinal images can lead to unsatisfactory results of automatic image processing, (such as segmentation and tracking), which may further affect disease analysis. A data-driven approach was proposed by Zhao et al. [42] to enhance the blurry retinal images in a weakly supervised manner, which can work on large image resolution and achieve a superior performance on blurry images. Considering the calculation performance and efficiency, we use traditional methods for image preprocessing. At the first of our work, we used grayscale conversion of images to reduce noise; then we used Z-score standardization and CLAHE to enhance the contrast of the image; and finally, we used Gamma calibration and data normalization to process data. The specific steps are as follows.

3.1.1. Gray conversion

The colored fundus image consists of grayscale images of three channels that are red, green, and blue [43]. Figure 3 shows the results when the color image was converted to a different channel. In Figure 3(a) the original color image, (b) the red channel image, (c) the green channel image, (d) the blue channel image. In order to better display the structural information of blood vessels in the fundus

image, in this study, we use the floating-point algorithm to convert a color image into a grayscale image. Compared with the single-channel grayscale image, the overall contrast of the converted grayscale image is higher, and almost no detail loss, which can better show the vascular structure of the fundus. As shown in Figure 5(b).

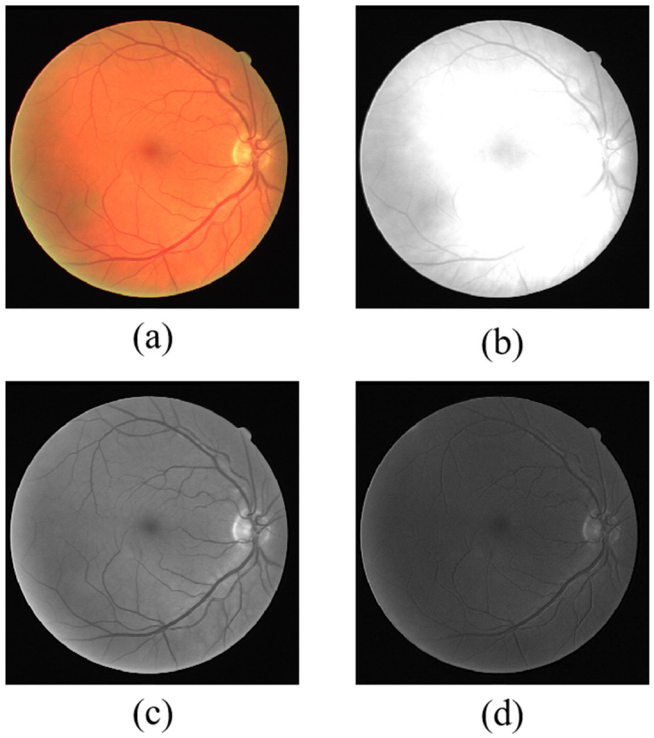

Figure 3. Grayscale image of three channels. (a) the original color image, (b) the red channel image, (c) the green channel image, (d) the blue channel image.

3.1.2. Z-score standardization

Z-score standardization normalizes the mean and variance of the original data and then transforms into unitless z-score scores, which could improve the comparability of the data. We normalized the mean and standard deviation of the grayscale image of the obtained fundus image, which makes the processed data conform to the normal distribution [44]. The mean is 0 and the standard deviation is 1. Our study uses z-score standardization, and the formula is defined as:

$$x_{new} = \frac{x - \mu}{\sigma} \tag{1}$$

Where x is image sample data, μ is the mean of the sample data, σ is the standard deviation of the sample data, and x_{new} is the image data output after normalization. As shown in Figure 5(c).

3.1.3. Contrast limited adaptive histogram equalization

In order to better carry out subsequent processing work, and improve low-contrast images, our

study further enhanced the retinal fundus image by using CLAHE. This algorithm is mainly used to deal with the problem of excessive amplification noise caused by Adaptive Histogram Equalization (AHE), while enhancing image contrast. First, the image is cut into 8 × 8 size areas called "titles", and then each "title" is processed by histogram equalization. CLAHE uses a predefined threshold to crop the histogram to limit the amplification. Typically, the cropped histogram is evenly distributed to other parts of the histogram. Figure 5(d) is a result picture after CLAHE processing.

3.1.4. Gamma calibration and normalization

Gamma calibration is used to adjust the intensity of image illumination, and is a non-linear operation. Normalization normalizes the image data, which we call linear transformation. The pixel values are distributed in the range of (0–1) to eliminate the influence of the dimension on the final result.

Gamma formula is defined as:

$$V_{out} = V^{\gamma} \tag{2}$$

Where V is the input image data, V_{out} is the output result, and γ is the value to be adjusted. Since the image data is automatically calibrated to the image during acquisition, the step is used to offset the effect of the device on image calibration. In our work, the value of γ is 1.2. We compared the results of the three cases ($\gamma = 0.9, 1.2, 1.5$), when γ is equal to 1.2, it can reduce the background noise without affecting the recognition of small blood vessels.

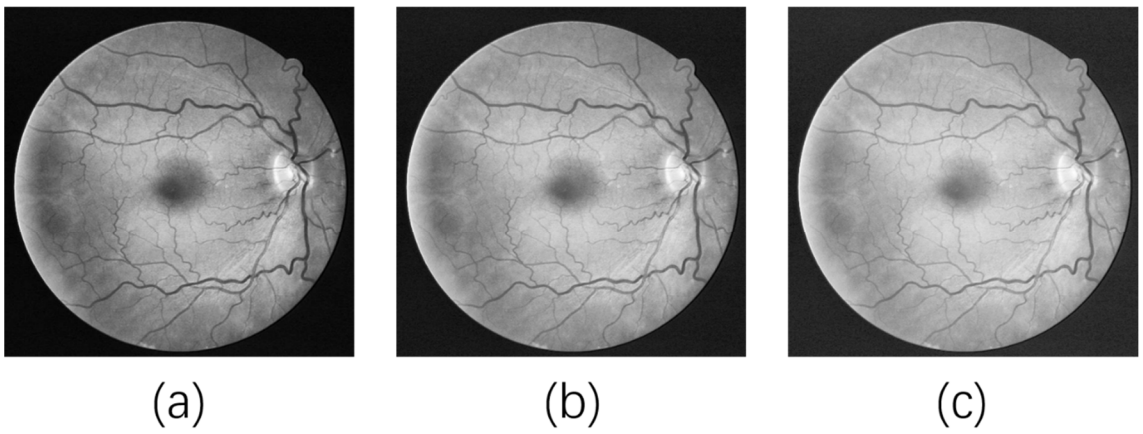

Figure 4. The results of different gamma value. (a) $\gamma = 0.9$, (b) $\gamma = 1.2$, (c) $\gamma = 1.5$.

Normalization formula is defined as follows:

$$x_{out} = \frac{x - x_{min}}{x_{max} - x_{min}} \tag{3}$$

Where x is the value of input image pixel, x_{min} is the minimum value in the sample data, x_{max} is the maximum value in the sample data, and x_{out} is the value of normalized pixel. Figure 5(e) shows the results of Gamma calibration and data normalization.

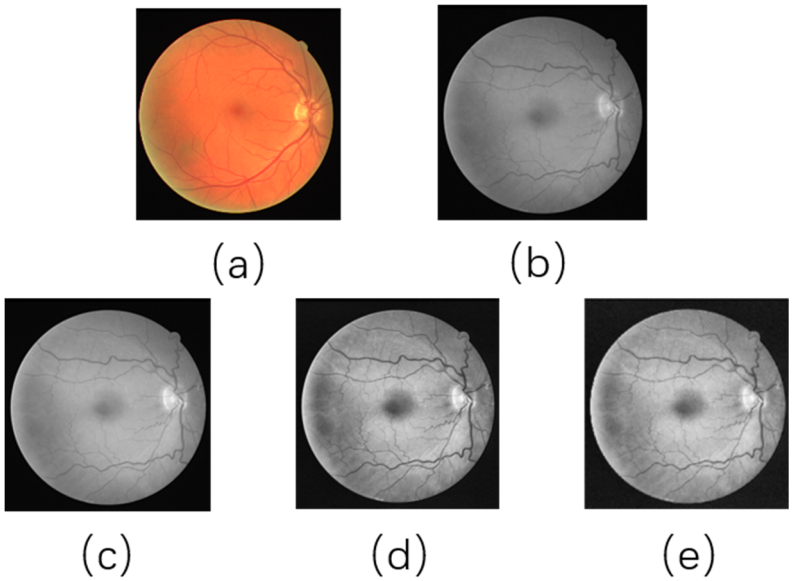

Figure 5. The pre-process of image. (a) Input image, (b) The image after gray conversion processing, (c) The image after z-score standardization processing, (d) The image after CLAHE processing, (e) The image after Gamma calibration and normalization processing.

3.2. U-shaped network

The fundus segmentation algorithm based on deep learning, in order to obtain better results, it is necessary to simultaneously retain the high-level semantic information of the image and the low-level detail information of the image [45]. However, for fundus vessels, such a small sample size makes it difficult to train a deep neural network. One way to solve this problem is to use a pre-trained network and then fine-tune it on the target data set. The other way is to use extensive data expansion and design a network architecture that can more efficiently preserve the high-level semantic information and the low-level details of images, e.g. U-Net [18].

U-Net is able to copy low-level features to corresponding advanced features, making signals spread between low and high levels in a simpler way. This not only compensates for low-level finer details to advanced semantic features, but also helps to improve the training efficiency of the model. In a way, this is similar to the idea of residual neural network. The residual neural network greatly improves the performance of the model by setting a bypass path. However, due to the small amount of fundus vascular image data, it is difficult to train a neural network that is too deep or too wide. Therefore, we introduce the dense block [46] based on Residual U-Net [47], by connecting the features learned from different layers, implementing feature reuse, reducing redundancy in the network, leveraging the potential of the network and yielding condensed models that are easy to train and highly parameter efficient. Results prove that the introduction of the dense block can effectively improve the performance of the U-Net model.

3.3. Improved and optimized U-shaped network-dense block

In order to solve the problem that the small blood vessels cannot be accurately segmented, the

proposed algorithm needs to be improved in terms of accuracy and sensitivity. The proposed U-Net network greatly promotes the research of medical image segmentation. U-Net network consists of a contraction path that gradually reduces the spatial dimension of the image by a downsampled operation, and a symmetric expanding path that gradually repairs the details and spatial dimensions of the object by upsampling operations.

In order to avoid the Vanishing gradient and over-fitting problems in U-Net, our study improved the network on the original U-Net. Adding a dense block to the U-Net forms a new architecture Dense U-Net model. As shown in Figure 6. The core idea of the dense block is that directly connect all layers under the premise of ensuring maximum information transfer between layers in the network. In other words, the input to each layer comes from the output of all the previous layers. Because of the existence of the dense block, the U-Net has a narrower network, fewer parameters, and better training results. The dense block formula is defined as follows:

$$X_i = H_i([X_0, \ldots\ldots, X_{i-1}]) \tag{4}$$

Where X_i is the input feature map of the ith layer, $X_0, \ldots\ldots, X_{i-1}$ is the connection of all the output feature maps of the 0 th layer to the $(i-1)$ th layer, and H_i identifies the nonlinear transformation. In order to solve the problem that too many network layers lead to poor network generalization ability, H_i also includes Batch Normalization (BN) [48], Rectified Linear Unit (ReLU) and 3 × 3 convolution. This study used the PReLU as the activation function. This function has a faster convergence speed without the problem of Vanishing gradient, and it also solves the case of "necrosis" of ReLU neurons. The formula is defined as follows:

$$\mathrm{PReLU(x)} = \begin{cases} \mathrm{x} & (\mathrm{x} > 0) \\ a\mathrm{x} & (\mathrm{x} \leq 0) \end{cases} \tag{5}$$

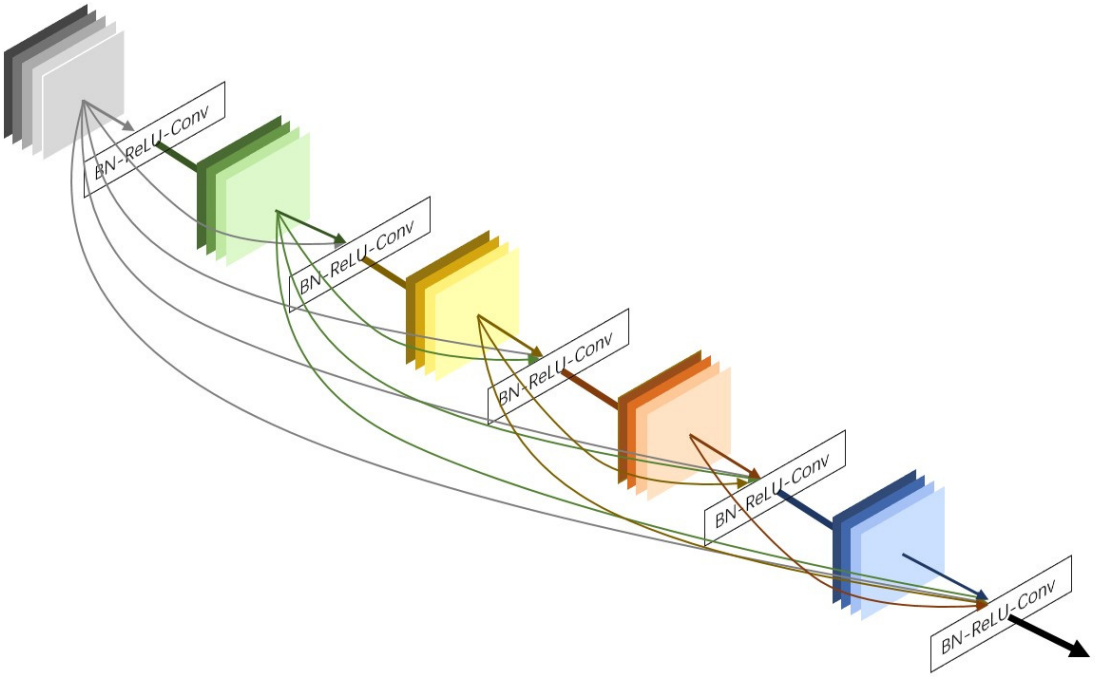

Figure 6. Dense block architecture diagram.

3.4. Dense U-Net retinal blood vessel segmentation network architecture model

Dense U-Net architecture proposed by our team is a neural network for semantic segmentation. This architecture combines the advantages of U-Net and Densely Connected Convolutional Networks. This combination enables the Dense U-Net to better transfer and combine the high-level semantic information and the low-level detail information, making full use of the feature map generated by each layer of the model, and reducing the redundancy of the model parameters.

Dense U-Net architecture is shown in Figure 7. The improved Dense U-Net architecture still uses U-Net's symmetric structure, including contraction path, bridge and symmetric expanding path. The contraction path includes three structural blocks, each structural block consists of a dense block, a transition block, and a downsampled, and is used to capture the context information of the image. Transition block consists of "BN + PReLU + 1 × 1 Conv". By introducing a 1 × 1 convolutional layer to reduce the number of feature maps can achieve cross-channel interaction and information integration, and improve computational efficiency. Bridge is composed of a dense block, a transition block, and an upsampling, and is used to connect the contraction path and the expansion path. The expansion path includes two structural blocks and a final output unit for accurately positioning the image segmentation region and implementing semantic segmentation. Each structural block of the expansion path is composed of a stitching layer, a dense block, a transition block, and an upsampling. After the final output unit passes through the stitching layer and the dense block, project a multi-channel feature map into a desired segmentation through a 1 × 1 convolution layer and a sotfmax activation layer. The main parameters of the model are as follows:

Table 1. Main parameters of Dense U-Net model.

	Block level	Dense block		Transition block	Output size
		Layer	Filter	Filter	
contracting path	Level 1	4	3 × 3/16	32	24 × 24 × 32
	Level 2	4	3 × 3/32	64	12 × 12 × 64
	Level 3	4	3 × 3/64	128	6 × 6 × 128
bridge	Level 4	4	3 × 3/128	256	12 × 12 × 256
expanding path	Level 5	4	3 × 3/64	128	24 × 24 × 128
	Level 6	4	3 × 3/32	64	48 × 48 × 64
	Level 7	4	3 × 3/16	–	48 × 48 × 2

AS: Contracting path: Level 1–3; bridge: Level 4; expanding path: Level 5–7. Dense block: Layer is the number of dense block; Filter is the number of filters. Eg: 3 × 3/16 means 16 filters whose size is 3 × 3.

Our model uses 'categorical_crossentropy' as the loss function, 'Stochastic Gradient Descent' as the optimizer. The learning rate of the model is 1×10^{-5}, the batch-size is 32, and the epoch is 200. The model is trained and validated on DRIVE and CHASE_DB1 dataset.

4. Materials and experiments

4.1. Dataset

DRIVE [27] (http://www.isi.uu.nl/Research/Databases/DRIVE/) and CHASE_DB1

(http://blogs.kingston.ac.uk/retinal/chasedb1) database is a public, common fundus image database. Most of the papers published today use these common databases to verify the performance of their proposed algorithms.

DRIVE fundus image dataset was built specifically to compare the effects of the blood vessel segmentation algorithm. The fundus images in this database are all from a diabetic fundus lesion screening organization. The images were from 400 diabetic subjects whose age is 25–90 years old and taken by a Canon 3CCD camera with a 45° field of view. DRIVE fundus image dataset was built by forty photographs which are randomly selected from 400 diabetic subjects. 33 of the dataset did not show any signs of diabetic retinopathy, and 7 showed signs of mild early diabetic retinopathy. The image in the database is in JPEG format. Our study experiment with the training set and test set that have been classified in the DRIVE database. The training set includes original images, standard vascular images manually segmented by experts, and fundus mask images. 20 pictures of each part are used for network training. Each part of the test set is also used 20 images for testing the effects of the training.

CHASE_DB1 [28] fundus image database contains 28 fundus images with a resolution of 999 × 960 pixels. The images of the database are collected from the left and right eyes of 14 children. In our study, the first 20 fundus images are used as the training set, and the remaining 8 fundus images are used as test sets.

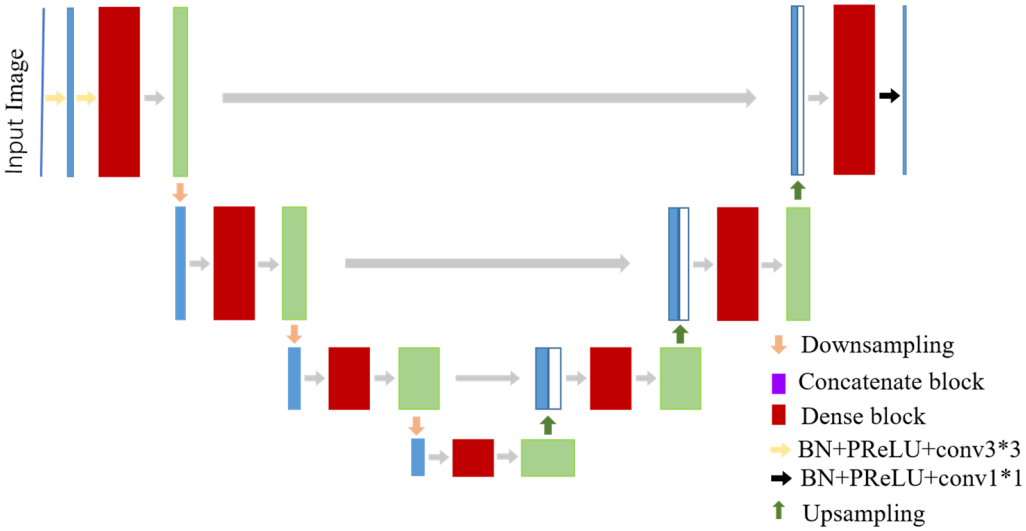

Figure 7. Dense U-Net architecture.

4.2. Experiments setting

We had experimented on the Drive and CHASE_DB1. The DRIVE dataset is consisted of 40 retinal images. Based on common experimental design ideas and data characteristics of the DRIVE dataset, we used 20 samples to train and remaining 20 samples to test. The size of each original image is 565 × 584 pixels. In this implementation, we considered 190,000 randomly selected patches from the images for training, where 171,000 patches are used for training, and the remaining 19,000 patches used for validation. As shown in Figure 8, we pick 40 patches to exhibit, the size of each patch is 48 × 48.

The CHASE_DB1 fundus image database contains 28 retinal images. The size of each original image is 999 × 960 pixels, we use 20 samples to train and remaining 8 samples to test as the dimensionality of the input data larger than the entire DRIVE dataset, we considered 300,000 randomly selected patches from 20 images for training.

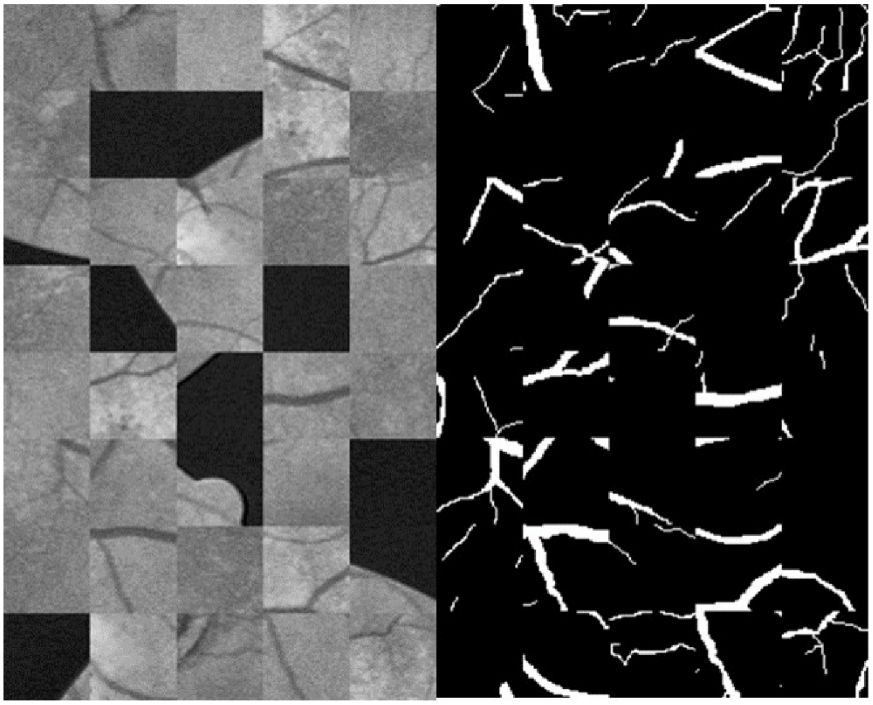

Figure 8. Left is the example patches with pre-processed and right is the corresponding outputs of patches.

4.3. Evaluation metrics

When segmenting the retinal fundus image, each pixel is classified into vascular and non-vascular. In order to evaluate the performance of the proposed algorithm, four metrics are used in this study: Specificity (Sp), sensitivity (Se), accuracy (Acc) and the area under the ROC curve (AUC). Se shows the proportion of correctly segmented blood vessel points to the sum of gold standard blood vessel points. Sp shows the proportion of the correctly segmented background points to the sum of the gold standard background points. Acc shows the proportion of correctly segmented pixels to the sum of the pixels of the entire image.

The calculation formula for each indicator is as follows:

$$\text{Se} = \frac{TP}{TP + FN} \tag{6}$$

$$\text{Sp} = \frac{TN}{TN + FP} \tag{7}$$

$$\text{Acc} = \frac{TP + TN}{TP + FN + TN + FP} \tag{8}$$

Where: True positive (TP) indicates that the blood vessel pixel is correctly classified as a vascular; false negative (FN) indicates that the blood vessel pixel is misclassified as a non-vascular; false positive (FP) indicates that the non-vascular pixel is misclassified as a vascular; true negative (TN) indicates that non-vascular pixels are correctly classified as non-vascular.

AUC is an important curve to measure the classification problem and the accuracy of vessel segmentation. In this study, AUC was calculated to judge the performance of the blood vessel segmentation. The closer the value of AUC is to 1, the better the performance of the corresponding blood vessel segmentation method.

4.4. Results from different datasets

The baseline algorithm used in this study is U-Net and Res-U-Net [49]. As shown in Table 2, the two datasets are presented in [49] and the methods presented in this study. The value of Sp and Acc produced by our proposed method on DRIVE dataset is better than the other two methods. On CHASE_DB1 data set, the value of Se is higher than the Res-U-Net architecture. As shown in the table, the value of AUC on DRIVE dataset and CHASE_DB1 dataset are both better than Res-U-Net, Which are 0.9793 and 0.9785 respectively.

Table 2. The result of DRIVE and CHASE_DB1.

Dataset	method	Sp	Se	Acc	AUC
DRIVE	U-Net [49]	0.9820	0.7537	0.9531	0.9755
	Res-U-Net [49]	0.9816	0.7751	0.9556	0.9782
	Proposed method	0.9834	0.7672	0.9559	0.9793
CHASE_ DB1	U-Net [49]	0.9701	0.8288	0.9578	0.9772
	Res-U-Net [49]	0.9820	0.7726	0.9553	0.9779
	Proposed method	0.9540	0.8967	0.9488	0.9785

AS: U-Net [49] and Res-U-Net [49] are baseline algorithms.

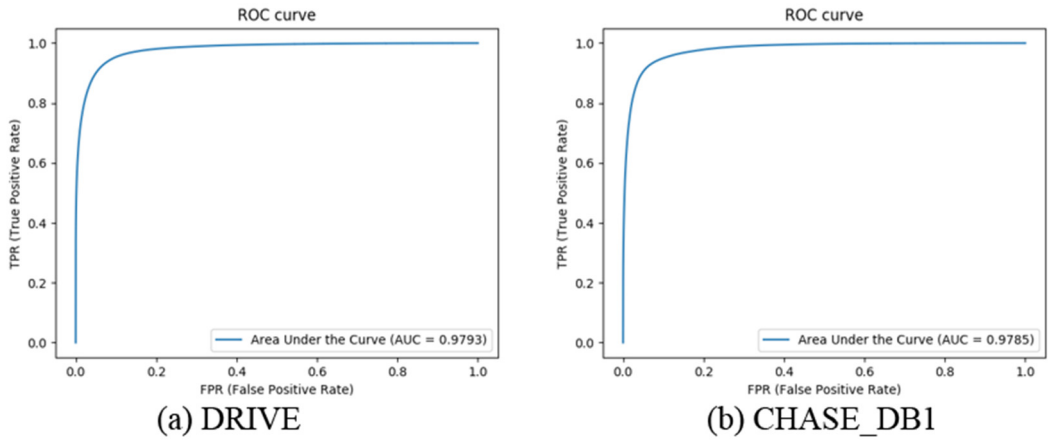

Figure 9. ROC curves for DRIVE and CHASE_DB1 datasets.

ROC curves for DRIVE, and CHASE_DB1 show as Figure 9. Extracting the pictures Randomly from the DRIVE and CHASE_DB1 databases are shown in Figures 10 and 11, respectively. As shown in these figures and the results in Table 2, it is clear that the proposed method has accurately detected and segmented the presence of blood vessels fundus in retinal images of all datasets.

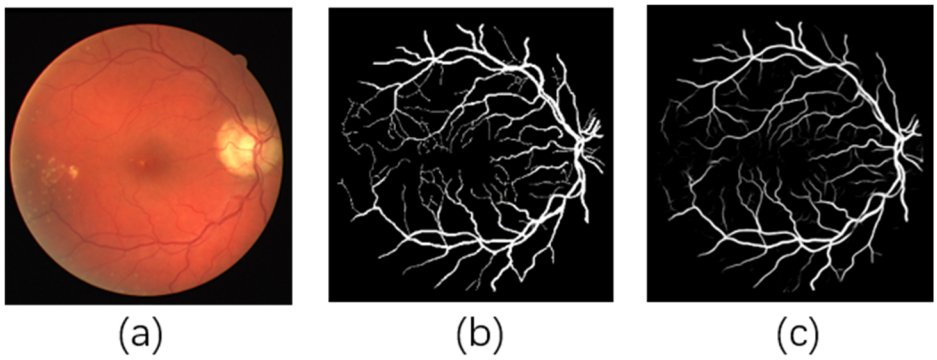

Figure 10. Vessel segmentation results for DRIVE database. (a) Input image, (b) 1st Human observer and (c) vessel segmentation by proposed method.

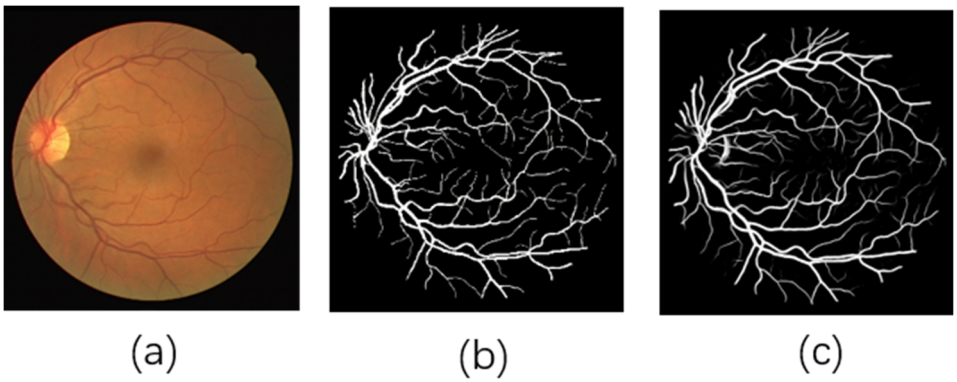

Figure 11. Vessel segmentation results for DRIVE database. (a) Input image, (b) 1st Human observer and (c) vessel segmentation by proposed method.

4.5. Comparison of the results of Dense U-Net and other methods

The performance of the proposed method is compared with the state-of-the-art methods in terms of the Se, Sp, Acc and AUC metrics on the DRIVE and CHASE_DB1 databases. As shown in the Table 3. The performance measurements of the comparison methods were taken directly from their respective publications.

On DRIVE dataset, our proposed method is superior to other methods in Sp, Acc, AUC, and slightly lower on Se. The effect on CHASE_ DB1 dataset is relatively poor, but it is the same as the performance of the state-of-the-art method basically, and there is still some lead in some performance. The value of Acc and AUC on DRIVE dataset obtained by our proposed method is 0.9559 and 0.9793, Compared to the state-of-the-art method, we have been achieved the best results so far.

The value of Acc and AUC on the CHASE_ DB1 dataset obtained by our proposed method is 0.9488 and 0.9785. The value of Acc is slightly lower than other algorithms by 0.01, but in the value of AUC, it is second only to the literature published in 2019 [50]. For retinal vascular segmentation problems, the quantitative measures of accuracy, sensitivity, specificity do not reflect true performance. In this article, we use AUC, which is a good indicator of the performance of the model. Simultaneously, the value of AUC in all the datasets obtained by our proposed method is 0.9793 and 0.9785. These results show that the algorithm of this study is superior to all algorithms on DRIVE dataset and is superior to most algorithms on CHASE_DB1 dataset.

Table 3. Comparison of proposed method with other methods.

Method	Year	DRIVE				CHASE_ DB1			
		Sp	Se	Acc	AUC	Sp	Se	Acc	AUC
Mendonca and Campilho [51]	2006	0.9764	0.7344	0.9452	–	–	–	–	–
Zhang et al. [32]	2010	0.9724	0.7120	0.9382	–	–	–	–	–
Fraz, Remagnino et al. [52]	2012	0.9807	0.7406	0.9480	0.9774	0.9711	0.7224	0.9469	0.9712
Azzopardi, Strisciuglio et al. [53]	2015	0.9704	0.7655	0.9442	0.9614	0.9587	0.7585	0.9387	0.9487
Li, Feng [54]	2016	0.9716	0.7569	0.9527	0.9738	0.9793	0.7507	0.9581	0.9716
Aslani and Sarnel [55]	2016	0.9801	0.7545	0.9513	0.9682	–	–	–	–
Y.Zhao, J.Zhao et al. [56]	2017	0.9790	0.7820	0.9570	0.8860	–	–	–	–
Hu, Zhang et al. [57]	2018	0.9793	0.7772	0.9533	0.9759	–	–	–	–
Alom [49]	2018	0.9813	0.7792	0.9556	–	–	–	–	–
Mahdi Hashemzadeh [50]	2019	0.9800	0.7830	0.9531	0.9752	0.9840	0.7737	0.9623	0.9789
Proposed method	2019	0.9834	0.7672	0.9559	0.9793	0.9540	0.8967	0.9488	0.9785

AS: Bold font is the best result.

In this chapter, we compared different results of different methods based on the architecture of U-Net. There is still a direction that we should care about it. The focus of our article is mainly on the architecture of U-Net. Compared with U-Net, some research work's focus is the improvement of dense network. Daniel Pelt and James Sethian proposed a mixed-scale dense network, which called MS-D Net [58]. MS-D Net is based on using dilated convolutions to capture features at different image scales and densely connecting all feature maps with each other. This kind of network can achieve better results in medical image segmentation task with fewer parameters and faster speed. Table 3 list the comparison of proposed method with other methods. These results are based on two datasets, DRIVE and CHASE_DB1. On the medical image segmentation task by using the dense net, the above two data sets have not yet been used for comparison. The comparison with the segmentation effect of dense networks will make our results more convincing. MS-D Net abandoned pooling operation and made each layer have a same size, which connected the dense layer conveniently. Theoretically, the efficiency of this network is better than our algorithm. Because in addition to considering the dense architecture, our algorithm also needs to consider the U-Net architecture, which also shows that our algorithm needs more time but has higher accuracy.

5. Conclusion

Retinal vascular segmentation of fundus images can prevent retinopathy of diabetic patients, and

can also reduce the prevalence of diseases. Retinal vascular segmentation of fundus images can also evaluate the treatment of eye diseases. Retinal blood vessel segmentation is usually performed based on two methods: Supervised and unsupervised. Up to now, many algorithms proposed based on these two methods have its advantages and disadvantages.

In this study, we proposed to form a new retinal vessel segmentation model by adding a dense block based on the U-Net network architecture. Due to the input of each layer coming from the output of all the previous layers, this new architecture enables the Dense U-Net to better transfer and combine the high-level semantic information and the low-level detail information, making full use of the feature map generated by each layer of the model, and reducing the redundancy of the model parameters.

In the training process, in order to solve the problems of over-fitting and learning efficiency, the batch normalization function (BN) and the PReLU activation function are used to optimize.

The segmentation performance of the existing algorithm model is compared on the public datasets DRIVE and CHASE_DB1 dataset. The model proposed in this study improves the accuracy of vascular segmentation, and also achieves better results for the segmentation of small blood vessels, such as retinal capillaries.

We should not only think about U-NET but also dense net which provides more possibilities for different segmentation scenarios. some applications pursue efficiency, and some pursue precision. The exploration of medical image segmentation tasks for dense networks is also our future work. In future work, on the one hand, it is necessary for us to compare the advantages and disadvantages of the two architectures, and on the other hand, to find more application scenarios of these two algorithms.

Acknowledgments

This research/work was supported by the National Key Research and Development Program of China [No. 2018YFC0116900, No. 2016YFC0901602], Key Research and Development Program of Guangdong [No.810229511112], National Natural Science Foundation of China (NSFC) [No. 61876194], Joint Foundation for the NSFC and Guangdong Science Center for Big Data [No. U1611261], Science and Technology Program of Guangzhou [No. 201604020016].

Conflict of Interest

The authors declare no competing financial interests.

Reference

1. S. Moccia, E. De Momi, S. El Hadji, L. S. Mattos, Blood vessel segmentation algorithms—review of methods, datasets and evaluation metrics, *Comput. Methods Programs Biomed.*, **158** (2018), 71–91.
2. H. K. Li, M. Horton, S. E. Bursell, J. Cavallerano, I. Zimmer-Galler, M. Tennant, Telehealth practice recommendations for diabetic retinopathy, *Telemed. E. Health*, **17** (2011), 814–837.
3. M. M. Fraz, P. Remagnino, A. Hoppe, B. Uyyanonvara, A. R. Rudnicka, G. C. Owen, et al., Blood vessel segmentation methodologies in retinal images–a survey, *Comput. Methods Programs Biomed.*, **108** (2012), 407–433.

4. F. Xu, X. C. Wang, M. Q. Zhou, Z. K. Wu, X. Y. Liu, *Segmentation algorithm of brain vessel image based on SEM statistical mixture model*, 2010 Seventh International Conference on Fuzzy Systems and Knowledge Discovery IEEE, 1830–1833. Available from: https://ieeexplore.ieee.org/abstract/document/5569429.
5. M. S. Hassouna, A. A. Farag, S. Hushek, T. Moriarity, Cerebrovascular segmentation from TOF using stochastic models, *Med. Image Anal.*, **10** (2006), 2–18.
6. D. A. Oliveira, R. Q. Feitosa, M. M. Correia, Segmentation of liver, its vessels and lesions from CT images for surgical planning, *Biomed. Eng. Online*, **10** (2011), 30.
7. E. Goceri, Z. K. Shah, M. N. Gurcan, Vessel segmentation from abdominal magnetic resonance images: Adaptive and reconstructive approach, *Int. J. Numer. Method Biomed. Eng.*, **33** (2017), e2811.
8. T. Mapayi, J. R. Tapamo, S. Viriri, Retinal vessel segmentation: A comparative study of fuzzy C-means and sum entropy information on phase congruency, *Int. J. Adv. Rob. Syst.*, **12** (2015), 133.
9. R. Nekovei, Y. Sun, Back-propagation network and its configuration for blood vessel detection in angiograms, *IEEE Trans. Neural Networks*, **6** (1995), 64–72.
10. J. V. Soares, J. J. Leandro, R. M. Cesar, H. F. Jelinek, M. J. Cree, Retinal vessel segmentation using the 2-D Gabor wavelet and supervised classification, *IEEE Trans. Med. Imaging*, **25** (2006), 1214–1222.
11. J. Staal, M. D. Abràmoff, M. Niemeijer, M. A. Viergever, B. Ginneken, Ridge-based vessel segmentation in color images of the retina, *IEEE Trans. Med. Imaging*, **23** (2004), 501–509.
12. S. Hanaoka, Y. Nomura, M. Nemoto, S. Miki, T. Yoshikawa, N. Hayashi, er al., *Hotpig: A novel geometrical feature for vessel morphometry and its application to cerebral aneurysm detection*, International Conference on Medical Image Computing and Computer-Assisted Intervention, 2015, 103–110. Available from: https://link.springer.com/chapter/10.1007/978-3-319-24571-3_13.
13. J. I. Orlando, E. Prokofyeva, M. B. Blaschko, A discriminatively trained fully connected conditional random field model for blood vessel segmentation in fundus images, *IEEE Trans. Biomed. Eng.*, **64** (2016), 16–27.
14. S. Chaudhuri, S. Chatterjee, N. Katz, M. Nelson, M. Goldbaum, Detection of blood vessels in retinal images using two-dimensional matched filters, *IEEE Trans. Med. Imaging*, **8** (1989), 263–269.
15. F. Zana, J. C. Klein, Segmentation of vessel-like patterns using mathematical morphology and curvature evaluation, *IEEE Trans. Image Process.*, **10** (2001), 1010–1019.
16. M. M. Fraz, S. A. Barman, P. Remagnino, A. Hoppe, A. Basit, B. Uyyanonvara, et al., An approach to localize the retinal blood vessels using bit planes and centerline detection, *Comput. Methods Programs Biomed.*, **108** (2012), 600–616.
17. Z. Jiang, H. Zhang, Y. Wang, S. B. Ko, Retinal blood vessel segmentation using fully convolutional network with transfer learning, *Comput. Med. Imaging Graphics*, **68** (2018), 1–15.
18. O. Ronneberger, P. Fischer, T. Brox, U-net: Convolutional networks for biomedical image segmentation; International Conference on Medical Image Computing and Computer-Assisted Intervention, 2015, 234–241. Available from: https://link.springer.com/chapter/10.1007/978-3-319-24574-4_28.
19. O. Oktay, J. Schlemper, L. L. Folgoc, M. Lee, M. Heinrich, K. Misawa, et al., Attention u-net: Learning where to look for the pancreas, *arXiv preprint arXiv:1804.03999* (2018).

20. L. Rundo, C. Han, Y. Nagano, J. Zhang, R. Hataya, C. Militello, et al., USE-Net: Incorporating Squeeze-and-Excitation blocks into U-Net for prostate zonal segmentation of multi-institutional MRI datasets, *Neurocomputing*, **365** (2019), 31–43.
21. X. C. Wang, W. Li, B. Y. Miao, H. Jing, Z. W. Jiang, W. Xu, et al., *Retina blood vessel segmentation using a U-net based Convolutional neural network*, International Conference on Data Science, 2018. Available from: https://researchbank.swinburne.edu.au/file/fce08160-bebd-44ff-b445-6f3d84089ab2/1/2018-xianchneng-retina_blood_vessel.pdf.
22. S. Kumawat, S. Raman, *Local Phase U-net for Fundus Image Segmentation*, ICASSP 2019 - 2019 IEEE International Conference on Acoustics, Speech and Signal Processing (ICASSP), 2019. 1209–1213. Available from: https://ieeexplore.ieee.org/abstract/document/8683390.
23. L. Xu, S. Luo, A novel method for blood vessel detection from retinal images, *Biomed. Eng. Online*, **9** (2010), 14.
24. S. L. Wang, Y. L. Yin, G. B. Cao, B. Z. Wei, Y. J. Zheng, G. P. Yang, Hierarchical retinal blood vessel segmentation based on feature and ensemble learning, *Neurocomputing*, **149** (2015), 708–717.
25. T. A. Soomro, A. J. Afifi, J. Gao, O. Hellwich, M. A. U. Khan, M. Paul, et al., *Boosting sensitivity of a retinal vessel segmentation algorithm with convolutional neural network*, 2017 International Conference on Digital Image Computing: Techniques and Applications (DICTA), 2017. Available from: https://ieeexplore.ieee.org/abstract/document/8227413/.
26. K. He, X. Zhang, S. Ren, J. Sun, *Delving deep into rectifiers: Surpassing human-level performance on imagenet classification*, Proceedings of the IEEE international conference on computer vision. 2015, 1026–1034. Available from: https://www.cv-foundation.org/openaccess/content_iccv_2015/html/He_Delving_Deep_into_ICCV_2015_paper.html.
27. T. A. Qureshi, M. Habib, A. Hunter, B. Al-Diri, *A manually-labeled, artery/vein classified benchmark for the DRIVE dataset*, Proceedings of the 26th IEEE International Symposium on Computer-Based Medical Systems, 2013. Available from: https://ieeexplore.ieee.org/abstract/document/6627847.
28. C. G. Owen, A. R. Rudnicka, R. Mullen, S. A. Barman, D. Monekosso, P. H. Whincup, et al., Measuring retinal vessel tortuosity in 10-year-old children: Validation of the computer-assisted image analysis of the retina (CAIAR) program, *Invest. Ophthalmol. Visual Sci.*, **50** (2009), 2004–2010.
29. F. Calimeri, A. Marzullo, C. Stamile, G. Terracina, Blood Vessel Segmentation in Retinal Fundus Images Using Hypercube NeuroEvolution of Augmenting Topologies (HyperNEAT); WIRN 2017, Quantifying and Processing Biomedical and Behavioral Signals, 173–183. Available from: https://link.springer.com/chapter/10.1007/978-3-319-95095-2_17.
30. M. G. Cinsdikici, D. Aydın, Detection of blood vessels in ophthalmoscope images using MF/ant (matched filter/ant colony) algorithm, *Comput. Methods Programs Biomed.*, **96** (2009), 85–95.
31. K. S. Sreejini, V. K. Govindan, Improved multiscale matched filter for retina vessel segmentation using PSO algorithm, *Egypt. Inf. J.*, **16** (2015), 253–260.
32. B. Zhang, L. Zhang, L. Zhang, F. Karraya, Retinal vessel extraction by matched filter with first-order derivative of Gaussian, *Comput. Biol. Med.*, **40** (2010), 438–445.
33. A. Hoover, V. Kouznetsova, M. Goldbaum, Locating blood vessels in retinal images by piecewise threshold probing of a matched filter response, *IEEE Trans. Med. Imaging*, **19** (2000), 203–210.

34. M. Vlachos, E. Dermatas, Multi-scale retinal vessel segmentation using line tracking, *Comput. Med. Imaging Graphics*, **34** (2010), 213–227.
35. F. K. Quek, C. Kirbas, Vessel extraction in medical images by wave-propagation and traceback, *IEEE Trans. Med. Imaging*, **20** (2001), 117–131.
36. B. S. Lam, Y. Gao and A. W. C. Liew, General retinal vessel segmentation using regularization-based multiconcavity modeling, *IEEE Trans. Med. Imaging*, **29** (2010), 1369–1381.
37. B. S. Y. Lam, H. Yan, A novel vessel segmentation algorithm for pathological retina images based on the divergence of vector fields, *IEEE Trans. Med. Imaging*, **27** (2008), 237–246.
38. L. Espona, M. J. Carreira, M. Penedo, M. Ortega, *Retinal vessel tree segmentation using a deformable contour model*, 2008 19th International Conference on Pattern Recognition, 2018. Available from: https://ieeexplore.ieee.org/abstract/document/4761762.
39. A. M. Reza, Realization of the contrast limited adaptive histogram equalization (CLAHE) for real-time image enhancement, *J. VLSI Signal Process. Syst. Signal Image Video Technol.*, **38** (2004), 35–44.
40. L. Rundo, A. Tangherloni, M. S. Nobile, C. Militello, D. Besozzi, G. Mauri, et al., MedGA: A novel evolutionary method for image enhancement in medical imaging systems, *Expert Syst. Appl.*, **119** (2019), 387–399.
41. M. Zhou, K. Jin, S. Wang, J. Ye, D. Qian, Color retinal image enhancement based on luminosity and contrast adjustment, *IEEE Trans. Biomed. Eng.*, **65** (2018), 521–527.
42. H. Zhao, B. Yang, L. Cao, H. Li, *Data-Driven Enhancement of Blurry Retinal Images via Generative Adversarial Networks*, Medical Image Computing and Computer Assisted Intervention–MICCAI 2019, 75–83. Available from: https://link.springer.com/chapter/10.1007/978-3-030-32239-7_9.
43. T. Kumar, K. Verma, A Theory Based on Conversion of RGB image to Gray image, *Int. J. Comput. Appl.*, **7** (2010), 7–10.
44. A. Jain, K. Nandakumar, A. Ross, Score normalization in multimodal biometric systems, *Pattern Recognit.*, **38** (2005), 2270–2285.
45. A. Elbalaoui, M. Fakir, K. Taifi, *A. Merbouha, Automatic detection of blood vessel in retinal images*, 2016 13th International Conference on Computer Graphics, Imaging and Visualization (CGiV), 2016. Available from: https://ieeexplore.ieee.org/abstract/document/7467731.
46. G. Huang, Z. Liu, L. Van Der Maaten, K. Q. Weinberger; *Densely connected convolutional networks*, The IEEE Conference on Computer Vision and Pattern Recognition (CVPR), 2017, 4700–4708. Available from: http://openaccess.thecvf.com/content_cvpr_2017/html/Huang_Densely_Connected_Convolutional_CVPR_2017_paper.html.
47. Z. Zhang, Q. Liu, Y. Wang, Road extraction by deep residual u-net, *IEEE Geosci. Remote Sens. Lett.*, **15** (2018), 749–753.
48. S. Ioffe, C. Szegedy, Batch normalization: Accelerating deep network training by reducing internal covariate shift, *arXiv preprint arXiv:1502.03167,* 2015.
49. M. Z. Alom, M. Hasan, C. Yakopcic, et al., Recurrent residual convolutional neural network based on u-net (r2u-net) for medical image segmentation, *arXiv preprint arXiv:1802.06955* (2018).
50. M. Hashemzadeh, B. A. Azar, Retinal blood vessel extraction employing effective image features and combination of supervised and unsupervised machine learning methods, *Artif. Intell. Med.*, **95** (2019), 1–15.

51. A. M. Mendonca, A. Campilho, Segmentation of retinal blood vessels by combining the detection of centerlines and morphological reconstruction, *IEEE Trans. Med. Imaging*, **25** (2006), 1200–1213.
52. M. M. Fraz, P. Remagnino, A. Hoppe, B. Uyyanonvara, A. R. Rudnicka, C. G. Owen, et al., An ensemble classification-based approach applied to retinal blood vessel segmentation, *IEEE Trans. Biomed. Eng.*, **59** (2012), 2538–2548.
53. G. Azzopardi, N. Strisciuglio, M. Vento, N. Petkova, Trainable COSFIRE filters for vessel delineation with application to retinal images, *Med. Image Anal.*, **19** (2015), 46–57.
54. Q. Li, B. Feng, L. Xie, P. Liang, H. Zhang, T. Wang, A cross-modality learning approach for vessel segmentation in retinal images, *IEEE Trans. Med. Imaging*, **35** (2015), 109–118.
55. S. Aslani, H. Sarnel, A new supervised retinal vessel segmentation method based on robust hybrid features, *Biomed. Signal. Process. Control*, **30** (2016), 1–12.
56. Y. Zhao, J. Zhao, J. Yang, Y. Liu, Y. Zhao, Y. Zheng, et al., Saliency driven vasculature segmentation with infinite perimeter active contour model, *Neurocomputing*, **259** (2017), 201–209.
57. K. Hu, Z. Zhang, X. Niu, Y. Zhang, C. Cao, F. Xiao, et al., Retinal vessel segmentation of color fundus images using multiscale convolutional neural network with an improved cross-entropy loss function, *Neurocomputing*, **309** (2018), 179–191.
58. D. M. Pelt, J. A. Sethian, A mixed-scale dense convolutional neural network for image analysis, *Proc. Natl. Acad. Sci. USA*, **115** (2018), 254–259.

AIMS Press